Study of magnetic and optical properties of $Zn_{1-x}TM_xTe$ (TM = Mn, Fe, Co, Ni) diluted magnetic semiconductors: First principle approach

Q Mahmood[1], M Hassan[1,†], and M A Faridi[2]

[1] Department of Physics, University of the Punjab, Quaid-e-Azam Campus-54590, Lahore, Pakistan
[2] Centre for High Energy Physics, University of the Punjab, Lahore, Pakistan

(Received 2 August 2016; revised manuscript received 19 November 2016; published online 20 December 2016)

We present structural, magnetic and optical characteristics of $Zn_{1-x}TM_xTe$ (TM = Mn, Fe, Co, Ni and $x = 6.25\%$), calculated through Wien2k code, by using full potential linearized augmented plane wave (FP-LAPW) technique. The optimization of the crystal structures have been done to compare the ferromagnetic (FM) and antiferromagnetic (AFM) ground state energies, to elucidate the ferromagnetic phase stability, which further has been verified through the formation and cohesive energies. Moreover, the estimated Curie temperatures T_c have demonstrated above room temperature ferromagnetism (RTFM) in $Zn_{1-x}TM_xTe$ (TM = Mn, Fe, Co, Ni and $x = 6.25\%$). The calculated electronic properties have depicted that Mn- and Co-doped ZnTe behave as ferromagnetic semiconductors, while half-metallic ferromagnetic behaviors are observed in Fe- and Ni-doped ZnTe. The presence of ferromagnetism is also demonstrated to be due to both the p–d and s–d hybridizations between the host lattice cations and TM impurities. The calculated band gaps and static real dielectric constants have been observed to vary according to Penn's model. The evaluated band gaps lie in near visible and ultraviolet regions, which make these materials suitable for various important device applications in optoelectronic and spintronic.

Keywords: magnetic semiconductors, density functional theory, optical and dielectric properties, electron density of states and band structure of crystalline solids

PACS: 75.50.Pp, 31.15.E–, 51.70.+f, 71.20.–b **DOI:** 10.1088/1674-1056/26/2/027503

1. Introduction

A wide range of theoretical and experimental reports, available in the literature, depict huge motivations to explore interesting materials for versatile device functionalities.[1–10] The semiconductors belonging to II–VI, III–VI, IV–VI, are extensively being explored for various applications. Particularly, the II–VI based DMSs, for example ZnS, ZnSe, and ZnTe, are considered to be attractive owing to their wide direct band gaps, which can offer versatile opto-electronic characteristics, therefore, could be expected to replace the existing silicon-based devices.[11–15] ZnTe crystallizes in zinc blende phase with a cubic lattice constant of 6.103 Å,[16] and the reported direct band gap is 2.26 eV,[17] which enables its application in the devices operable at high temperatures and power levels. ZnTe has attracted huge attention because of its low cost, large absorption coefficient, and higher solubility to magnetic impurities without significant structural deteriorations.[18,19]

The undoped and doped ZnTe in thin film, nanoparticle, and bulk forms have been fabricated and characterized with various experimental techniques.[20–25] For example, thin films of $Zn_{1-x}Ni_xTe$ (x_{Ni} up to 20%), deposited on glass substrate by employing electron beam evaporation, have demonstrated that with the increasing Ni content, the band gap and micro strains are reduced, while the grain size is improved, which depict that Ni impurity ions may induce optical and structural modifications.[26] The nanocrystals of Mn-doped ZnTe synthesized by hot injection method have shown that the emission band centered at 620 nm, corresponds to narrow absorption bands for different crystal sizes, which confirmed that emission is due to Mn^{+2} substituted ZnTe.[27] Similarly, the Co-doped ZnTe prepared by thermal diffusion method has depicted that Co doping shifts the absorption edge towards the lower energy, and optical transitions of the electrons to the dopant induced states are considered to be responsible for the observed absorption lines.[28] Another report about Fe-doped ZnTe ($x_{Fe} = 0.867$ and 1.21%)) crystals grown by Bridgman technique have shown that from the optical data the values of the exchange constants $N_0\alpha$ and $N_0\beta$ can be qualitatively realized. The computed exchange constants agree well with the already reported values.[29] In spite of a number of experimental reports on optical properties of transition metal (TM) doped ZnTe, no comprehensive experimental study about the magnetic and optical properties exists.

The ZnTe has widely been explored by using the density functional theory (DFT). In a previous report on ZnTe doped with 25% Fe, Ni, Co, samples have exhibited half-metallicity due to Fe and Ni doping, while semiconducting properties are attained due to Co doping.[30] The results are found to be consistent with a previous comprehensive theoretical study, in which Cr, Fe and Ni doping in ZnTe results in a

†Corresponding author. E-mail: mahmood.physics@pu.edu.pk

© 2017 Chinese Physical Society and IOP Publishing Ltd

half-metallic character, while Co and Mn depict semiconducting behavior.[31] The half-metallic ferromagnets (HMFMs), in which one sub-band show metallic nature, while the other sub-band exhibit insulating behavior, and the semiconducting materials, in which both sub-bands show insulating behaviors, are crucial for novel spintronic applications.[31,32] Moreover, Mn- and V-doped ZnTe have also been investigated by Wein2K package and it observed that for $x_{\mathrm{Mn}} = 12.5\%$, ground state stabilizes with antiferromagnetic nature, while reducing Mn content to $x_{\mathrm{Mn}} = 6.25\%$ induces a ferromagnetic ground state, which is in agreement with the experiments.[30] However, no experimental or theoretical study about systematic investigation of TM-doped ZnTe is available.[33–36] The experimentally determined magnetic characteristics, as well as the theoretically investigated optical properties are limited in the literature, particularly, at the low impurity concentrations.[37,38]

In this study, we report a comprehensive investigation of structural, electronic, magnetic and optical properties exhibited by $\mathrm{Zn}_{1-x}TM_x\mathrm{Te}$ (TM = Fe, Ni, Co, Mn and $x = 6.25\%$). In order to get the most accurate electronic band structure and energy band gap, E_{g}, that approach experimental values, we have used modified Becke–Johnson (mBJ) functional. Therefore, the calculated opto-electronic and magnetic properties are expected to bear close resemblance to the experimentally measured behaviors, which enables one to accurately simulate and explore the fundamental and applied materials' phenomena, hence, elucidates the precision and worth of the presented theoretical investigations. The computed Curie temperatures (T_{c}) have shown that compounds exhibit above room temperature ferromagnetism (RTFM). Moreover, the optical properties of this material system have also been reported and have been found to be highly sensitive to the structural, electronic and magnetic properties.

2. Method of calculations

Various novel material characteristics[39–41] can be elucidated by employing various theoretical methods.[42–44] In the present study, we have used FP-LAPW method, which is implemented in Wein2K software,[45] to compute the structural and electronic characteristics of $\mathrm{Zn}_{1-x}TM_x\mathrm{Te}$ (TM = Fe, Ni, Co, Mn and $x = 6.25\%$). In FP-LAPW technique, the unit cell is considered to be composed of non-overlapping spheres, which are separated by the interstitial regions. We have used a supercell of 32 atoms for the zinc blende ZnTe (space group: 216 ($F43m$)) with Wyckoff positions of Zn and Te atoms as $(0,0,0)$ and $(0.25,0.25,0.25)$, respectively. The impurities addition results in a change in the space group of the host ZnTe lattice to 111 (P-42m). The generalized gradient approximation (GGA),[46] as suggested by Wu and Cohen, is employed to reveal the exchange–correlation (XC) effects. Additionally, modified Becke and Johnson (mBJ)[47] potential is employed to determine the most accurate electronic band characteristics, particularly, the band gap, E_{g}, which is consistent with the experiment. The presented results are computed at the ground state lattice constants, which are extracted from the Murnaghan equation of state.

In order to control the plane-wave expansion, the convergence parameter represented as $R_{\mathrm{MT}} \times K_{\mathrm{max}}$, ($R_{\mathrm{MT}}$ represents the smallest radius of the MT spheres, while K_{max} indicates the cutoff for the plane-wave), is taken as 7.0. The maximum values of the angular momentum, I_{max}, is taken as 10. To avoid the charge leakage, the separation between core and valence states is defined in terms of energy cut-off parameter, which is adjusted to -6.0 Ry (1 Ry = 13.6057 eV). The 1000 k-points have been used for the sampling the reciprocal space. The energy convergence up to 0.01 mRy is achieved by a set of repeated iterations.

3. Results and discussions

3.1. Structural stability

The realization of a stable Zn-based diluted magnetic semiconductors (DMS) phase is a controversial topic being widely explored. Sato *et al.*[48] have shown that spin glass phase is present in $\mathrm{Zn}_{1-x}TM_x\mathrm{Te}$ (TM = Fe, Co, and Ni) DMSs, while antiferromagnetic behavior has been reported for Mn-doped ZnTe. Moreover, the nanostructured single phase $\mathrm{Zn}_{0.97}\mathrm{Mn}_{0.03}\mathrm{Te}$ has simultaneously exhibited paramagnetism, ferromagnetism and superparamagnetism. The observed room temperature ferromagnetism in $\mathrm{Zn}_{0.97}\mathrm{Mn}_{0.03}\mathrm{Te}$ has been reported to be induced by the bound magnetic polarons (BMP).[49] In another study, p-type ferromagnetism is exhibited due to weakly localized holes in Mn-doped ZnTe, according to Zener/RKKY interaction.[50] In contrast, electron spin resonance (ESR) and magnetic susceptibility studies indicated the stability of the paramagnetic state at room temperature (RT).[51] Therefore, in order to elucidate the actual stable phase, we have employed the relaxed structure in the ferromagnetic (FM) as well as in the antiferromagnetic (AFM) phase, to calculate the ground state energies of TM-doped ZnTe DMS. The positive ΔE ($\Delta E = E_{\mathrm{AFM}} - E_{\mathrm{FM}}$) have indicated a higher FM state stability (see Table 1). Further confirmation about the FM state is demonstrated through the formation energy (ΔH), which has been extracted using the following equation.[52]

$$\Delta H = E_{\mathrm{Total}}\left(TM_l\mathrm{Zn}_m\mathrm{Te}_n\right) - lE_{TM} - mE_{\mathrm{Zn}} - nE_{\mathrm{Te}}, \quad (1)$$

where $E_{\mathrm{Total}}\left(TM_l\mathrm{Zn}_m\mathrm{Te}_n\right)$ represent the total ground state (GS) energy of TM-doped (TM = Mn, Fe, Co, Ni) ZnTe DMSs, while E_{TM}, E_{Zn}, and E_{Te} are the GS energies of bulk elements in a unit cell. The subscripts l, m, n, respectively, represent the number of TM, Zn, and Te ions in each unit cell

volume. The formation energies exhibit negative sign (see Table 1) which indicates that energy releases during compound formation, elucidating stability in FM state. Moreover, the TM doping causes higher energy release, in contrast to the experimental value (−28.10 eV)[53] for ZnTe, as shown in Table 1. Hence, TM dopants enhance the phase stability, which is an additional advantage. The stability of $Zn_{1-x}TM_xTe$ compounds is also confirmed from the cohesive energy (E_{coh}) that binds the atoms together in the crystal. The E_{coh} is computed by employing the following equation

$$\Delta E_{coh} = lE_{TM}^{atom} + bE_{Zn}^{atom} + cE_{Te}^{atom} - E_{Total}(TM_aZn_bTe_c). \quad (2)$$

Here $E_{Total}(TM_aZn_bTe_c)$ is the total ground state energy of the compound and E_{TM}^{atom}, E_{Zn}^{atom}, and E_{Te}^{atom} are the ground state energies of isolated atoms of TM, Zn, and Te, respectively. The cohesive energy of the pure ZnTe is in close match with that observed experimentally.[53] The cohesive energies of TM-doped ZnTe exhibit greater values than their binaries that again indicate FM state stability. In addition, both the formation and cohesive energies have been observed to increase from Mn to Ni, because increasing number of electrons in the d-shell increases binding between nucleus and electrons, therefore, stability of $Zn_{1-x}TM_xTe$ DMSs increases.

Table 1. Enthalpy of formation ΔH_f (eV), ground state energy ΔE (meV), Curie temperature T_c (K), cohesive energy (E_{coh}), direct exchange splitting energy $\Delta_x(d)$, indirect exchange splitting energy $\Delta_x(pd)$, exchange constants ($N_0\alpha$ and $N_0\beta$), the total magnetic moment per unit cell, magnetic moment on TMs site, magnetic moment on Te-site, band gap (E_g), half metallic band gap (G_{HM}), static dielectric constant $\varepsilon_1(0)$, and refractive index $n(0)$ calculated for $Zn_{0.9375}TM_{0.0625}Te$ (TM = Mn, Fe, Co, Ni).

Composition	Exp.	ZnTe	ZnMnTe	ZnFeTe	ZnCoTe	ZnNiTe
ΔH_f/eV	–28.10[a]	–	–94.08	–95.22	–94.19	–94.64
ΔE/meV	–	–	4.10	3.72	4.41	3.10
T_c/K	–	–	494	453	417	380
E_{coh}	4.48[a]	4.55	5.90	5.95	6.04	6.25
($\Delta E_{crystal}$)			2.07	1.33	2.92	0.86
$\Delta_x(d)$			3.07	2.14	5.33	3.02
$\Delta_x(pd)$			–0.80	–0.79	–0.57	–0.53
$N_0\alpha$			–0.217	0.236	–0.256	0.483
$N_0\beta$			–0.874	–0.925	–0.943	–1.086
Total MM			5.00	4.00	3.00	2.00
TM-site			4.245	2.572	2.423	1.313
Zn-site			0.254	0.345	0.311	0.232
Te-site			0.122	0.134	0.121	0.251
E_g	2.39[b]	2.39	2.32	2.37	2.36	2.32
G_{HM}	–	–	–	0.05	–	0.14
$\varepsilon_1(0)$	7.30[c]	6.70	6.77	7.14	9.00	28.6
$n(0)$	2.57[c]	2.58	2.62	2.67	3.00	5.41

[a]Ref. [53], [b]Ref. [54], [c]Ref. [55]

Moreover, Heisenberg model has been employed to estimate the Curie temperature of $Zn_{1-x}TM_xTe$ compounds by using the expression $T_c = 2\Delta E/3xK_B$, where x represents impurity cation concentration and K_B shows Boltzmann constant.[56] The estimated T_c values for Ni- and Mn-doped ZnTe, as listed in Table 1, have been observed to exhibit highest and lowest T_c, respectively. However, all the $Zn_{1-x}TM_xTe$ compounds have shown T_c above room temperature (RT), which already has been experimentally confirmed for $Zn_{1-x}Mn_xTe$ ($x = 1\%$).[57] Therefore, the studied DMSs are most suitable for spintronic device applications, which also indicate that experimental material properties can efficiently be simulated by employing theoretical methods.[58–60]

3.2. Electronic and magnetic behavior

The modified Becke–Johnson potential (mBJ) along with generalized gradient approximation (GGA) are utilized to find the most accurate band structures (BS) as well as the precise density of states (DOS) in $Zn_{1-x}TM_xTe$ ($x = 6.25\%$ and TM = Mn, Fe, Co, Ni) compounds, as presented in Figs. 1 and 2, respectively. The band gap computed for ZnTe is equal to that observed experimentally,[51] as is evident in Table 1, which confirms the accuracy of the presented calculations. The Mn- and Co-doped ZnTe have demonstrated a direct band gap at the Γ-point in the spin-up case, while in the spin-down channel, the states move to lower energy because of the p–d exchange splitting. Therefore, Fe- and Ni-doped ZnTe show a band gap around the E_F in the spin-up case, while in the spin-down case a metallic nature is evident due to the valence states crossing the E_F. Therefore, it is evident from Figs. 1–2 that the Mn–Co-doped ZnTe compounds are ferromagnetic semiconductors, while Fe–Ni-doped ZnTe compounds are half-metallic ferromagnets (HMFM), indicating a possibility of tuning the transport properties in ZnTe by varying the nature of dopant.

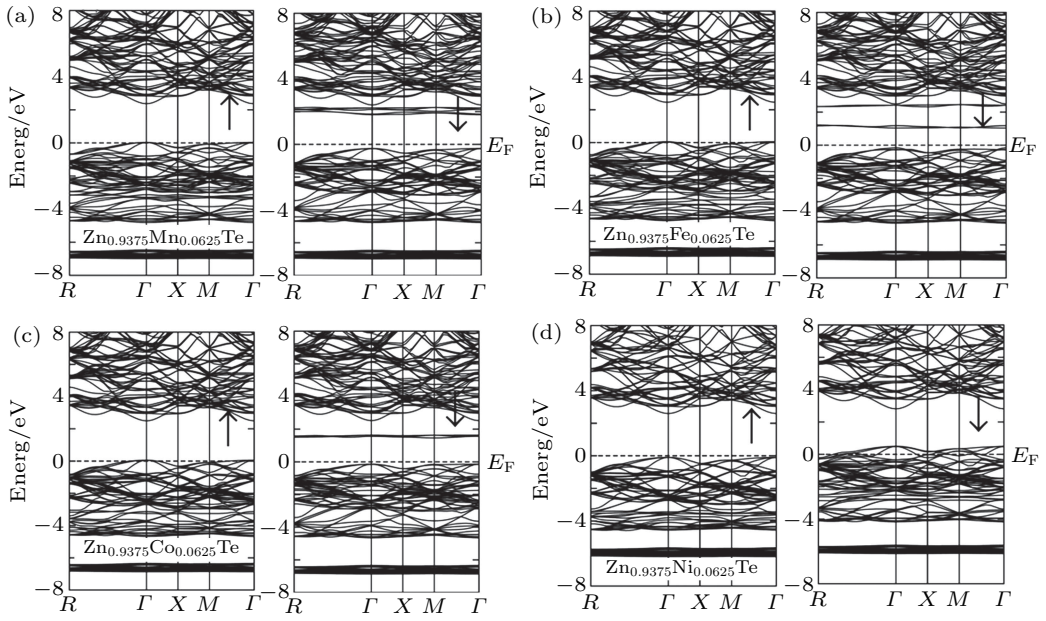


Fig. 1. The band structure for both spin-up and spin-down channels plotted for (a) $Zn_{0.9375}Mn_{0.0625}Te$, (b) $Zn_{0.9375}Fe_{0.0625}Te$, (c) $Zn_{0.9375}Co_{0.0625}Te$, (d) $Zn_{0.9375}Ni_{0.0625}Te$, calculated by employing mBJ-GGA functional.

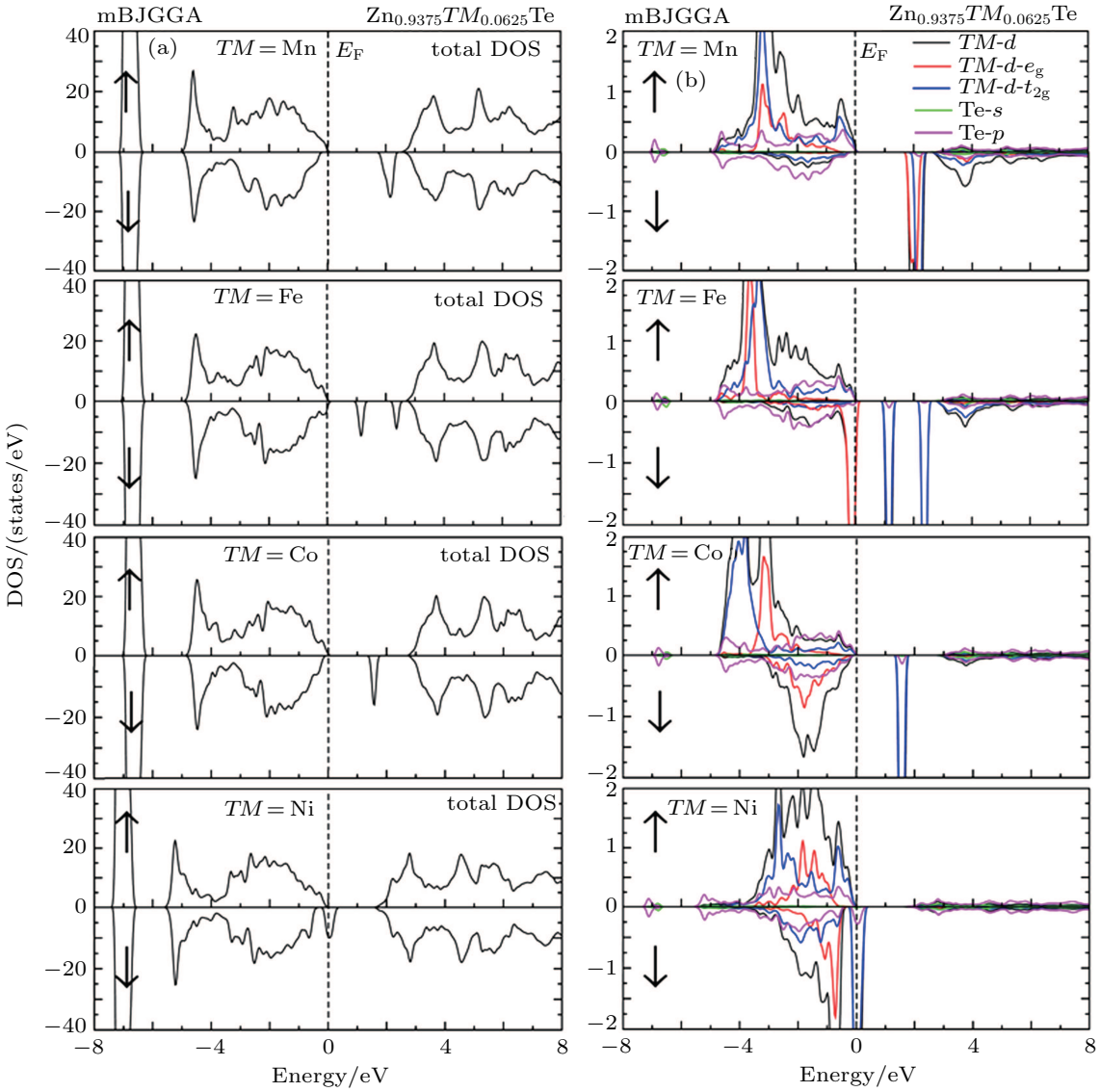


Fig. 2. (color online) (a) The total (TDOS) and (b) partial density of states (PDOS) plotted for $Zn_{0.9375}TM_{0.0625}Te$ (TM = Mn, Fe, Co, Ni), for both spin-up and spin-down channels and calculated by employing mBJ-GGA functional.

The real cause of the appearance of ferromagnetism has been investigated through the calculated partial density of states (PDOS), as presented in Fig. 2(b), and it has been found that ferromagnetism arises due to hybridization between TMs 3d-states and anion (Te) p-states. The studied compounds have shown strong p–d exchange interaction within the valence band of ZnTe to induce a p-type carrier induced ferromagnetism. The large exchange splitting occurs from Mn to Ni, which is due to the increasing number of d-electrons (Mn-3d^5, Fe-3d^6, Co-3d^7, Ni-3d^8). Furthermore, the tetrahedral environment formed by the Te anions produce a crystal field that is responsible for splitting 3d-states of the TMs into two states of e_g (d_{z^2}, $d_{x^2-y^2}$) and three states of t_{2g} (d_{xy}, d_{yz}, d_{zx}). Only d–t_{2g} states participate in hybridization, while e_g states do not take part. Moreover, the energy difference between e_g and t_{2g} states expresses the magnitude of the crystal field energy ($E_{cry} = E_{t_{2g}} - E_{e_g}$). The direct exchange splitting energy extracted from the position of TMs 3d-states in both spin-up and spin-down cases ($\Delta_x(d) = d^{\downarrow} - d^{\uparrow}$) in ZnTe has been observed to have larger magnitude compared to the crystal field splitting energy ($\Delta_x(d) > E_{cry}$) and, therefore, confirms the stability of ferromagnetic state (see Table 1 and Fig. 3).

In addition, during hybridization, the Mn and Co doping produce deficiency of electrons to induce hole-mediated ferromagnetism similar to that observed in GaMnAs, as is already explained by Zener.[61] In Fe- and Ni-doped ZnTe, the interaction arising between 3d-state of Fe/Ni impurities and p-states of host lattice Te anions, causes the appearance of the localized states within the band gap at E_F, which induce half-metallic ferromagnetic characteristics. Therefore, the large splitting of t_{2g} states causes the double exchange mechanism that is responsible for producing ferromagnetism in Fe- and Ni-doped ZnTe half-metallic semiconductors.

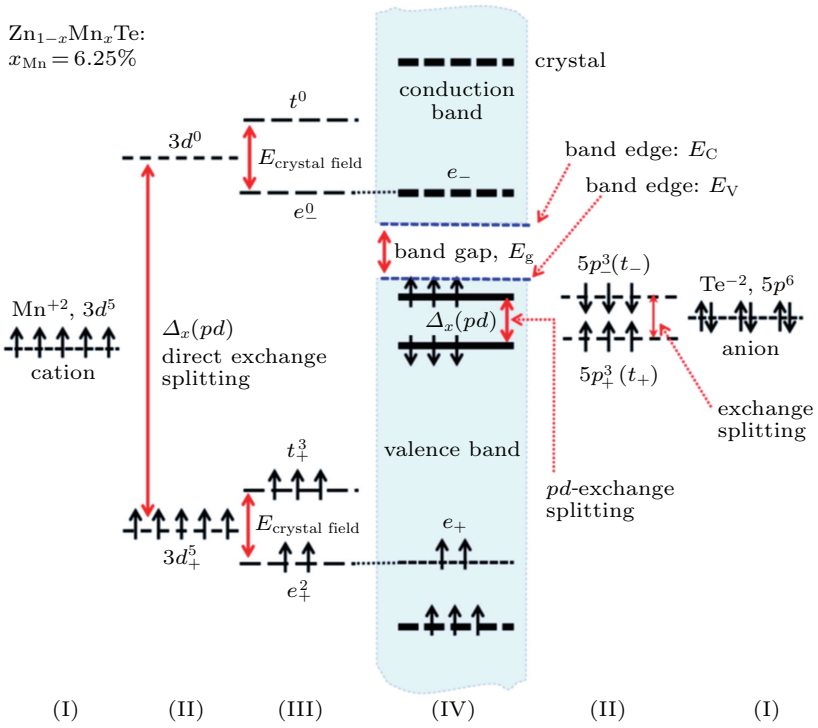


Fig. 3. (color online) The illustration of p–d repulsion model in $Zn_{1-x}Mn_xTe$. (I) Atomic magnetically polarized energy levels of Mn cation and host lattice Te anion, (II) exchange splitting of the energy levels $\Delta_x(d)$, (III) further splitting of the Mn-3d energy levels due to the crystal field, (VI) p–d exchange splitting $\Delta_x(p-d)$, due to the interaction between Mn-3d and Te-5p energy levels, the shaded area shows host lattice valence and conduction band. The figure description is followed by the reference.[59]

Another parameter about exchange splitting energy is $\Delta_x(pd)$, which is very important because its negative value shows that the p–d hybridization in the valence band is strong enough to realize a more attractive spin-down channel. The p–d repulsion model is used to justify the observed ferromagnetism, as is presented in Fig. 3, which is followed by the reference.[62] The exchange interaction appearing between anion p-states and cation 3d-states is responsible for splitting the states near the Fermi level E_F, which results in band broadening effects. In $Zn_{1-x}Mn_xTe$, the 3d-states of Mn split into five lower energy states $3d^5_+$ and five higher energy $3d^0_-$ states (see Fig. 3-II). The five $3d^5_+$ states further divided into two e_+ and three t_+ energy states. Similarly, $3d^0_-$ states also split into two e_- and three t_- energy states (see Fig. 3-III). On the other hand, the $5p^6$states of Te split into six energy states, three are lower energy states $3p^3_+(t_+)$, while three $3p^3_-(t_-)$ are at high energy, as shown in Fig. 3-II from the right side. Therefore, the repulsion model depicts that $\Delta_x(d) > E_{crystal}$, which evidences the presence of stable ferromagnetic state, as already explained above. Finally, the interaction between lower

(t_+^3 and $5p_+^3$) and higher energy states (t_-^0 and $5p_-^3$) causes the valence band to create an exchange energy gap ($\Delta_x(pd)$ in spin-down channel (see Fig. 3-VI). The negative value of $\Delta_x(pd)$ indicates p-type ferromagnetism, which decreases as TM dopant in ZnTe changes from Mn to Ni (see Table 1). Moreover, e_+ and e_- do not take part in hybridization as they are lower in energy, as depicted in Fig. 3-III.[63]

The number of unpaired electrons in $3d$-state of TMs contributes to the observed magnetic moment. It is interesting to observe that Mn^{2+} ($3d^5$) has five unpaired electrons (two in e_g state and three in t_{2g}), Fe^{2+} ($3d^6$) has four unpaired electrons (one in e_g state and three in t_{2g}), Co^{2+} ($3d^7$) has three unpaired t_{2g} electrons and Ni^{2+} ($3d^8$) has two unpaired t_{2g} electrons in their outermost shells, which are responsible for inducing free space magnetic moments.[64] Furthermore, the strong interaction between p-states of Te and dopant d-states reduces the free space magnetic moment of TM atoms by generating a significant amount of magnetic moments on Zn and Te sites,[65] as is depicted in Table 1. The positive sign of magnetic moment on anion and cation sites represents a ferromagnetic coupling.

In addition, the exchange constants, $N_0\alpha$ and $N_0\beta$ have also been calculated, which play a significant role in elucidating the real origin of ferromagnetism in DMSs. The Hamiltonian $H = -N_0\beta s.S$ of the system can be retrieved from these exchange constants, in which β represent the p–d exchange integral, while S and s are the TM impurity and hole carriers spin, respectively.[66,67] The $N_0\alpha$ and $N_0\beta$ are calculated from the following relations

$$N_0\alpha = \frac{\Delta E_C}{x\langle S\rangle} \quad \text{and} \quad N_0\beta = \frac{\Delta E_V}{x\langle S\rangle}, \tag{3}$$

Here x shows TM ion concentration, $\langle S\rangle$ is the average value of magnetic moment on TM ion site, $\Delta E_C = E_C^{\downarrow} - E_C^{\uparrow}$ and $\Delta E_V = E_V^{\downarrow} - E_V^{\uparrow}$ are the splitting at conduction and valence band edges, respectively. From Table 1, it is clear that the $N_0\alpha$ and $N_0\beta$ have anti-ferromagnetic coupling for Fe- and Ni-doped ZnTe compounds. While a ferromagnetic coupling for Mn- and Co-doped ZnTe compounds has been observed. The reason behind this anomaly can be explained in terms of valence and conduction band edge splittings. The kinetic exchange splitting at valence band maximum (VBM) results in large and negative $N_0\beta$, while small and positive $N_0\alpha$ appears at the conduction band minimum (CBM) because of the direct exchange splitting to generate half metallic ferromagnetic behavior. In FM semiconductors, the sign of $N_0\alpha$ is strongly influenced by crystal symmetry and may have higher magnitude arising due to the quantum confinement. During the splitting process at CBM, it has been noted that d level lies below the CBM in the minority spin channel, due to which, the CBM in the minority and majority channels, respectively, will energetically be moved down and up and that results in negative $N_0\alpha$. On the other hand, half-metallic ferromagnetic semiconductors have been observed to have the d-levels lying below the CBM, for both the majority and minority channels. Hence, d-level is pushed up to the CBM toward high energy in both minority and majority spin,[68] which causes positive $N_0\alpha$, as shown by the values presented in Table 1. Using the Heisenberg model, the Curie temperatures have also been predicted, which are 494, 453, 417, and 380 K for Mn-, Fe-, Co-, and Ni-doped ZnTe, respectively. The decrease in magnetic moment per magnetic ion from 5 μ_B to 2 μ_B by changing dopant from Mn to Ni causes a reduction in the magnitude of the exchange interactions and corresponding Tc reduces. Therefore, all the studied compounds can be used in various magnetic devices operating above room temperature.

3.3. Optical properties

The wide range of potential applications of Zn-based II–VI DMSs in the field of optoelectronics indicates that they may replace the silicon-based semiconductor technology. The calculated complex dielectric constant $\varepsilon(\omega) = \varepsilon_1(\omega) + i\varepsilon_2(\omega)$ can efficiently elucidate the optical responses shown by any material system. The $\varepsilon_2(\omega)$ is the imaginary part of the complex dielectric function that indicates absorption of light, while the real part $\varepsilon_1(\omega)$ can be determined by employing the imaginary part, by using the Kramer–Kronig relations,[69] which elucidates the scattering of electromagnetic radiations from the material surface. For achieving the complete details of the demonstrated optical properties by Mn-, Fe-, Co-, and Ni-doped ZnTe, we have plotted the various optical parameters in the energy range 0–25 eV, as depicted in Fig. 4. The $\varepsilon_1(\omega)$, which illustrates the quantitative measurement of the polarization induced in the material due to incident light, can be used to determine the static part of $\varepsilon_1(\omega)$, represented as $\varepsilon_1(0)$. The computed $\varepsilon_1(0)$, for un-doped ZnTe, closely matched with the experimental value,[55] as illustrated in Table 1. Moreover, it is evident in Fig. 4(a) and Table 1, the static value $\varepsilon_1(0)$ calculated from the $\varepsilon_1(\omega)$ spectra and the band gap of the studied materials are related exactly according to the Penn's model $\varepsilon_1(0) \approx 1 + (\hbar\omega_p/E_g)^2$.[70] The ω_p and E_g represent the plasma frequency and the material band gap, respectively. From Table 1, it can be observed that the studied materials exhibit a band gap between visible to ultraviolet regions of the electromagnetic spectrum that confirm the material's suitability to be employed in various optoelectronic devices. The value of $\varepsilon_1(0)$ increases as the magnetic ions change from Mn to Ni into ZnTe lattice, because electrons in the transition metal d-states increases. The $\varepsilon_1(\omega)$ reaches a peak value at 4 eV and drops to zero around 5 eV for Mn-, Fe-, Co-, and

Ni-doped ZnTe. In addition, $\varepsilon_1(\omega)$ depicts negative value between 5 eV to 15 eV (see Fig. 4(a)), indicating a total reflection of light from the surface, and as a result, a metallic characteristic arises.[71] The reason behind the observed metallic effect may be the zero band gap exhibited by the materials for this particular energy region. Therefore, incompatibility of the band gap with the incident photon energy causes a complete reflection, because only those electromagnetic radiations are absorbed, which have energy equal or greater than the material band gap.

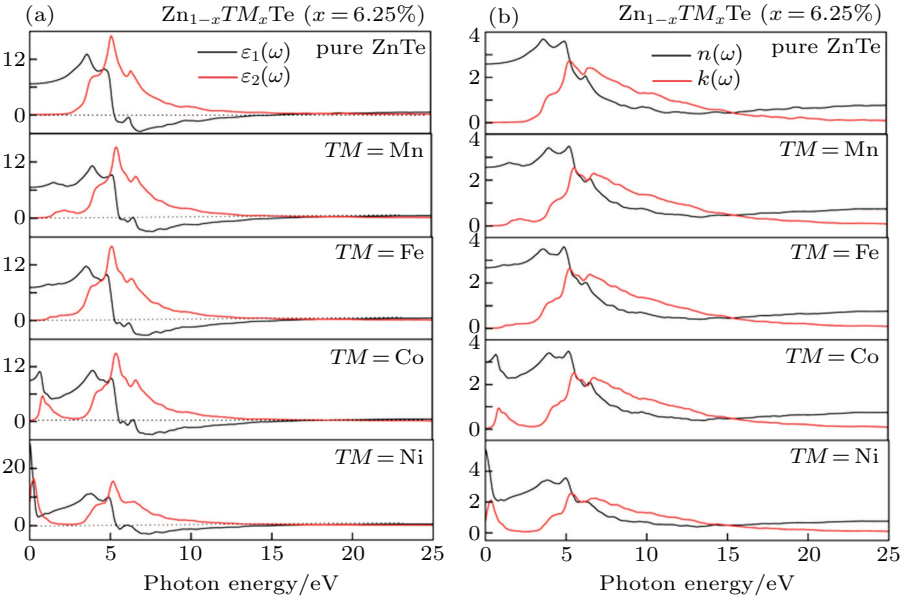


Fig. 4. (color online) (a) The real $\varepsilon_1(\omega)$ and imaginary part $\varepsilon_2(\omega)$ of the dielectric constant, (b) refractive index $n(\omega)$ and extension coefficient $k(\omega)$ plotted against incident energy for $Zn_{0.9375}TM_{0.0625}Te$ (TM = Mn, Fe, Co, Ni), and calculated by using mBJ-GGA functional.

The imaginary part $\varepsilon_2(\omega)$ of the complex dielectric constant is a key parameter to decide a suitable material for a suitable optoelectronic device. The $\varepsilon_2(\omega)$, as plotted in Fig. 4(a), shows that transition metal doping increases the width of the absorption region and peaks become less sharp compared to that for pure ZnTe. The critical values of $\varepsilon_2(\omega)$ illustrate the optical band gap of the materials, which is compatible with the band gap calculated from band structures (see Fig. 1) and, therefore, confirm the accuracy of our results. It is also evident in Table 1 that the band gap of TMs-doped alloys is less than the band gap of the un-doped ZnTe host semiconductor, which is due to increased number of electrons in the TM d-shell that reduces the effective distance between the atomic states. In DMSs, the strong p–d hybridization creates shallow levels just above the valence band for the realization of p-type semiconductors and below the conduction band for inducing n-type semiconductors, which can also contribute to the direct transitions from VB to the CB. Therefore, the band gap of a material decreases and a red shift takes place. As shown in Fig. 4(a), within the energy range 3 eV–8 eV, the large values of the $\varepsilon_2(\omega)$ peak intensities confirm that the studied materials have a maximum absorption in the near visible to ultraviolet region, which is important for optoelectronic technology. However, the $\varepsilon_2(\omega)$ in Ni-doped ZnTe alloy is quite different between 0 eV–1.5 eV, the $\varepsilon_2(\omega)$ starts from a higher value and then reduces to a minimum at higher energy. Similarly, a small peak in the energy region 0 eV–1.3 eV in Co-doped ZnTe may arise due to the free charge carriers produced due to Co doping.[72]

The refractive index $n(\omega)$ and the extinction coefficient $k(\omega)$ have also been computed and have depicted a behavior similar to $\varepsilon_1(\omega)$ and $\varepsilon_2(\omega)$, respectively (see Fig. 4). All four parameters are inter-related through the equations, $n^2 - k^2 = \varepsilon_1$, and $2nk = \varepsilon_2$. The static values of $n(0)$ and $\varepsilon_1(0)$ are in accordance with the relationship, $n_0^2 = \varepsilon_1(0)$, as is evident in Table 1. Moreover, the $n(0)$ for un-doped ZnTe finds an excellent match with the experiment[55] as demonstrated in Table 1. The $n(\omega)$, which illustrates the propagation and dispersion of the constituent wavelengths of light while crossing a medium, have shown large number of peaks within 4 eV–8 eV that disappear at higher photon energies. Therefore, the materials demonstrate the capability to absorb high-energy photons indicating the transparency of Mn-, Fe-, Co-, Ni-doped ZnTe alloys to low energy. Moreover, in the energy region 8 eV–25 eV, the value of $n(\omega)$ becomes fractional, showing that the group velocity ($v_g = c/n$, where n and c represent refractive index and speed of light, respectively) is greater than the speed of light ($c = \lambda\nu$, where ν is the frequency of incident radiations). Therefore, the group velocity indicates that the material exhibits a negative domain to demonstrate a nonlinear behavior, where the studied materials can be designed to act like a superluminal medium in which both permittivity and permeability due to the plasma resonance frequency become negative. The extinction coefficient k (ω) also measures

the absorption of light similar to $\varepsilon_2(\omega)$. Its value is maximum between 4 eV–8 eV and decreases to zero at the higher electromagnetic energy. The overall analysis of optical properties of the studied materials show that they absorb maximum in the near visible to UV and the critical values of the refractive indices vary between 2 eV to 5 eV. These two factors make the studied materials potential candidates for applications in optoelectronic devices.

4. Conclusion

The structural, magnetic and optical properties of $TM =$ Mn-, Fe-, Co-, Ni-doped ZnTe DMSs have been studied by using first principle calculations. The positive energy difference between AFM and FM states has verified the FM state stability, compared to the AFM state. The stability in the FM state has also been confirmed by negative value of enthalpy of formation and greater values of the cohesive energy for TM-doped DMSs than the binary un-doped ZnTe host semiconductor. The Curie temperature has also been predicted from the Heisenberg classical model, which shows above room temperature ferromagnetism (RTFM). It has been shown that the Mn and Co doping in ZnTe induces ferromagnetic semiconducting nature, while Fe and Ni doping in ZnTe reveals half-metallic ferromagnetic character. In addition, the ferromagnetism has also been confirmed from the negative values of the exchange splitting energy $\Delta_x(pd)$ and exchange constant $N_0\beta$. The higher value of direct exchange energy $\Delta_x(d)$ than the crystal field energy also evidences the presence of stable FM states. Moreover, the magnetic moment of TMs has been found to decrease by inducing small magnetic moments on the nonmagnetic sites which is due to the strong p–d hybridization. The optical properties of $TM =$ Mn-, Fe-, Co-, Ni-doped ZnTe DMSs have also been calculated to explore potential optical applications. The static value of dielectric constants and optical band gaps are observed to vary according to the Penn's model indicating the accuracy of the presented calculations. It has been noted from the imaginary part of the dielectric constant that the studied materials are red-shifted with maximum absorption in the visible as well as in the ultraviolet energy. Therefore, the studied compounds are the best candidates for optoelectronic and spintronic devices.

Acknowledgment

One of the authors Mahmood-ul-Hassan (M Hassan) is grateful to the University of the Punjab, Lahore for financial support through faculty research grant program. This paper is part of the Ph. D. thesis submitted by Qasim Mahmood (Q Mahmood) to the University of the Punjab, Lahore.

References

[1] Zhang W and Huang J 2016 *Chin. Phys. B* **25** 057103
[2] En-Ge W and Wang M 2011 *Adv. Search. Chin. J. Lab. Medicine* **40** 333
[3] Ai L Q, Zhang X X, Chen M and Xiong D X 2016 *Acta Phys. Sin.* **65** 096501 (in Chinese)
[4] Hao C 2007 *Adv. Search. Chin. J. Lab. Medicine* **36** 910
[5] Al-Khateeb, Alqadi M K, Alzoubi, Albiss B, Hasan M K and Ayoub N Y 2016 *Chin. Phys. B* **25** 058402
[6] Zhang W W, Hu M, Liu X, Li N and Yan W J 2016 *Acta Phys. Sin.* **65** 090701 (in Chinese)
[7] Xiong Y 2016 *Chin. Phys. Lett.* **33** 057402
[8] Ru-Shan H 2010 *Adv. Search. Chin. J. Lab. Medicine* **39** 753
[9] Zhang Y, Duan L, Ji V and Xu K W 2016 *Chin. Phys. B* **25** 058102
[10] Xie Q Y, Zhai Z Y, , Chen G B, Wu X S and Gao J 2016 *Chin. Phys. Lett.* **33** 56103
[11] Tamargo M C, Brasil M J S P, Nahory R E, Martin R J, Weaver A L and Gilchrist H L 1991 *Semicond. Sci. Technol.* **6** A8
[12] Su C H, Feth S, Volz M P, Matyi R, George M A, Chattopadhyay K, Burger A and Lehoczky S L 1999 *J. Cryst. Growth* **207** 35
[13] Prinz G A, Jonker B T, Krebs J J, Ferrari J M and Kovanic F 1986 *Appl. Phys. Lett.* **48** 1758
[14] Eryong N, Donglai L, Yusen Z, Xue B, Liang Y, Yong J, Zhifeng J and Xiasong S 2011 *Appl. Surf. Sci.* **257** 8762
[15] Kim Y D, Cooper S L and Klein M V 1993 *Appl. Phys. Lett.* **62** 2387
[16] Hellwege K H and Madelung O 1982 *Numerical Data and Functional Relationships in Science and Technology* (New York: Springer-Verlag)
[17] Ibrahim A, El-Sayed N, Kaid M and Ashour A 2004 *Vacuum* **75** 189
[18] Haury A, Wasiela A, Arnoult A, Cibert J, Tatarenko S, Dietl T and Merle daubigne Y 1997 *Phys. Rev. Lett.* **79** 511
[19] Ferrand D, Cibert J, Bourgognon C, Tatarenko S, Wasiela A, Fishman G, Bonanni A, Sitter H, Kolesnik S, Jaroszynski J, Barcz A and Dietl T 2000 *J. Cryst. Growth* **214/215** 387
[20] Mahmood Q, Murtaza G, Ahmad R, Hussain T and Will I G 2016 *Curr. Appl. Phys.* **16** 361
[21] Erlacher A, Ambrico M, Perna G, Schiavulli L, Ligonzo T, Jaeger H and Ullrich B 2005 *Appl. Surf. Sci.* **248** 402
[22] Wang W, Ni C, Zhu T, Zhang H and Xiao J Q 2006 *J. Appl. Phys.* **99** 08D503
[23] Hou X J, Teo K L, Sreenivasan M G, Liew T and Chong T C 2006 *Thin Solid Films* **505** 126
[24] Tang F L, Su H L, Chuang P Y, Wu Y C, Huang J C A, Huang X L and Jin Y 2014 *RSC Adv.* **4** 49308
[25] Mahmood A, Rashid R, Aziz U, Shah A, Ali Z, Raza Q and Ashraf T 2015 *Prog. Nat. Sci.: Mater. Int.* **25** 22
[26] Eilers J, Groeneveld E, Donega C M and Meijerink A 2012 *J. Phys. Chem. Lett.* **3** 1663
[27] Vaksman Y F, Nitsuk Y A, Pavlov V V, Purtov Y N, Nasibov A S and Shapkin P V 2007 *Semiconductors* **41** 660
[28] Testelin C, Prost J B, Menant M, Zielinski M and Mycielski A 2000 *Solid State Commun.* **113** 695
[29] Mahmood Q, Hassan M, Faridi M A, Sabir B, Murtaza G and Mahmood A 2016 *Curr. Appl. Phys.* **16** 549
[30] Guo M, Gao G and Hu Y 2011 *J. Magn. Magn. Mater.* **323** 122
[31] McNorton R D, Schuler T M and MacLaren J M 2008 *Phys. Rev. B* **78** 075209
[32] Katsnelson M I, Yu-Irkhin V, Chioncel L, Lichtenstein A I and de Groot R 2008 *Rev. Mod. Phys.* **80** 315
[33] Dowben P A and Skomski R 2004 *J. Appl. Phys.* **95** 7453
[34] Sato K and Yoshida H K 2001 *Hyperfine Interactions* **136/137** 737
[35] Ueda S, Sekiyama A, Iwasaki T, Imada S, Suga S, Saitoh Y, Giriat W and Takeyama S 2008 *Phys. Rev. B* **78** 205206
[36] Benkhettou N and Bensaid D 2008 *J. Conden. Matt. Phys.* **29** 290301
[37] Zaari H, Boujnah M, El Hachimi A, Benyoussef A and El Kenz A 2014 *Opt. Quantum Electron.* **46** 75
[38] Wang Q, Sun Q and Jena P 2005 *J. Appl. Phys.* **97** 043904
[39] Xia C J, Zhang B Q, Yang M, Wang C L and Yang A Y 2016 *Chin. Phys. Lett.* **33** 47101
[40] Zhao Z Y, Wang H L and Li M 2016 *Acta Phys. Sin.* **65** 097101 (in Chinese)
[41] Lee W C and Wu C 2016 *Chin. Phys. Lett.* **33** 037201
[42] Wu H and Li F 2016 *Acta Phys. Sin.* **65** 096801 (in Chinese)
[43] Zhu X H, Chen X R and Liu B 2016 *Chin. Phys. B* **25** 057501
[44] Zhang H H, Li X D, Xie Y P, Hu L J and Yao M Y 2016 *Acta Phys. Sin.* **65** 096802 (in Chinese)

[45] Blaha P, Schwarz K, Madsen G K H, Kvasnicka D and Luitz J 2001 "WIEN2K: An Augmented-Plane-Wave + Local Orbitals Program for Calculating Crystal Properties", Karlheinz Schwarz, Techn. Wien, Austria
[46] Wu Z and Cohen R E 2006 *Phys. Rev. B* **73** 235116
[47] Tran F and Blaha P Phys. 2009 *Rev. Lett.* **102** 226401.
[48] Sato K and Yoshida H K 2001 *J. Appl. Phys.* **40** L651
[49] Tang F L, Su H L, Huang S Y, Wu Y C, Huang J C A, Du Y W, Huang X L and Jin Y 2014 *J. Alloys Compd.* **617** 322
[50] Kepa H, Khoi L V, Brown C M, Dietl T, Furdyna J K and Giebultowicz T M 2004 *Physica B* **350** 36
[51] Rao N M, Vijayalakshmi R P, Reddy D R and Reddy B K 2008 *Spect. Acta Part. A* **69** 688
[52] Wei S H and Zunger A 1986 *Phys. Rev. B* **35** 2340
[53] Harrison W A 1989 "Electronic Structure and the Properties of Solids, the Physics of the Chemical Band", Stanford University
[54] Okuyama H, Kishita Y and Ishibashi A 1998 *Phys. Rev. B* **57** 2257
[55] Kootstra F, de Boeij P L and Snijders J C 2000 *Phys. Rev. B* **62** 7071
[56] Zhang C W and Yan S 2010 *J. Appl. Phys.* **107** 043913
[57] Fang W, Liu Y, Gou B, Peng L, Zhong Y, Zhang Z and Zhao Z 2014 *J. Alloys Compd.* **584** 240
[58] Wang H 2016 *Chin. Phys. Lett.* **33** 057802
[59] Tao X, Zhon-Yi L, Miao G and Xun-Wang Y 2011 *Adv. Search. Chin. J. Lab. Medicine* **40** 584
[60] Wang J, Zhang P and Duan X M 2016 *Chin. Phys. B* **25** 057301
[61] Dietl T, Ohno H, Matsukura F, Cibert J and Ferrand D 2000 *Science* **287** 1019
[62] Wei S H and Zunger A 1987 *Phys. Rev. B* **5** 2340
[63] Jaffe J E and Zunger A 1984 *Phys. Rev. B* **29** 1882
[64] Mahmood Q, Javed A, Murtaza G, Alay-e-Abbas S M 2015 *Mater. Chem. Phys.* **162** 831
[65] Xie J 2010 *J. Magn. Magn. Mater.* **322** L37
[66] Gaj G A, Planel R and Fishman G 1979 *Solid State Commun.* **29** 435
[67] Sanvito S, Ordejon P and Hill N A 2001 *Phys. Rev. B* **63** 165206
[68] Dalpian G M and Wei S H 2006 *Phys. Rev. B* **73** 245204
[69] Marius G 2010 *Kramers–Kronig relations (The Physics of Semiconductors)* (Berlin, Heidelberg: Springer)
[70] Penn D 1962 *Phys. Rev. B* **128** 2093
[71] Benstaalia W, Bentata S, Abbad A and Belaidi A 2013 *Mater. Sci. Semicond. Proc.* **16** 231
[72] Jeetendra S, Nagabhushana H, Mrudula K, Naveen C S, Raghu P and Mahesh H M 2014 *J. Electro-Chem. Sci.* **9** 2944